Scattering Phenomena in the Millimeter Wave (6G+) Range

A Major Qualifying Project
submitted to the Faculty of
WORCESTER POLYTECHNIC INSTITUTE
in partial fulfillment of the requirements for the
degree of Bachelor of Science in Physics
by Yifan Gu

Date:
28 April 2022

Project Advisor:
Prof. Douglas Petkie

Abstract:

The paper studies the diffraction behavior of the millimeter-wave by illuminating a cylindrical metallic rod with 60, 90, and 120 GHz Gaussian beams to investigate what would its diffraction image look like. For each frequency, the diffraction was repeated with four different distances between the rod and the detector, i.e., 9.5, 22, 31, and 39.5 cm. The author employed Igor Pro to plot all diffraction patterns using the data collected by the detector attached to a rotary stage, analyzed these patterns by computing their corresponding Fresnel numbers, and suggested future works based on the finding.

Acknowledgements

I would like to thank Jacob Bouchard for guiding me through setting up the experiment in the lab. Most importantly I would like to thank my advisor Prof. Doug Petkie for his help and insight and for countless hours spent in and out of the lab working with me.

Table of Contents

1. Introduction

The extraordinary progression of wireless devices nowadays induces an exponentially growing demand for higher data rates and service quality in networks [1,2]. The employment of millimeter-wave spectrum, i.e., 30~300 GHz, provides a solution to such a situation following its low cost and its ability to provide large continuous bandwidths that ensure data rates of multi-gigabits per second [1,3]. In particular, the millimeter-wave spectrum has attracted tremendous commercial interest in devices such as wireless communication and imaging system due to the IEEE 802.11ad standard [1,3,4]. One of the major applications of the millimeter-wave in imaging is the car radar system [2]. In order to recognize whether there is an object in front of the car for collision warning during driving on a highway, it is of paramount significance to know what the millimeter-wave will behavior when it hits an objective in front of it. In other words, we need to study and understand the diffraction behavior of the millimeter-wave if we want to put it into practice.

The primary goal of this project is to develop an experimental system to investigate the diffraction patterns of millimeter waves using 60, 90, and 120 GHz Gaussian beams and to validate the system by studying the diffraction from a cylindrical metallic rod. With this goal in mind, the remainder of the paper is structured as follows: the background chapter provides a brief and easy-following introduction to the core theories and concepts on which the diffraction experiment is founded; the methodology chapter explains the setting-up and the rationale of the rod diffraction experiment; the finding chapter exhibits and analyzes the results and data collected from the experiment; and the conclusion section summarizes the key findings and suggests the future work. All in all, it is the author's sincere wish that this paper can serve as a good reference to those audiences who are interested in the topic of millimeter wave and be the basis of future studies.

2. Background

2.1 Gaussian Beam

A Gaussian beam occurs when an electromagnetic wave that is confined to a specific diameter diverges out with an angle θ as it moves along the propagation axis (z-axis) as shown in Fig.1.

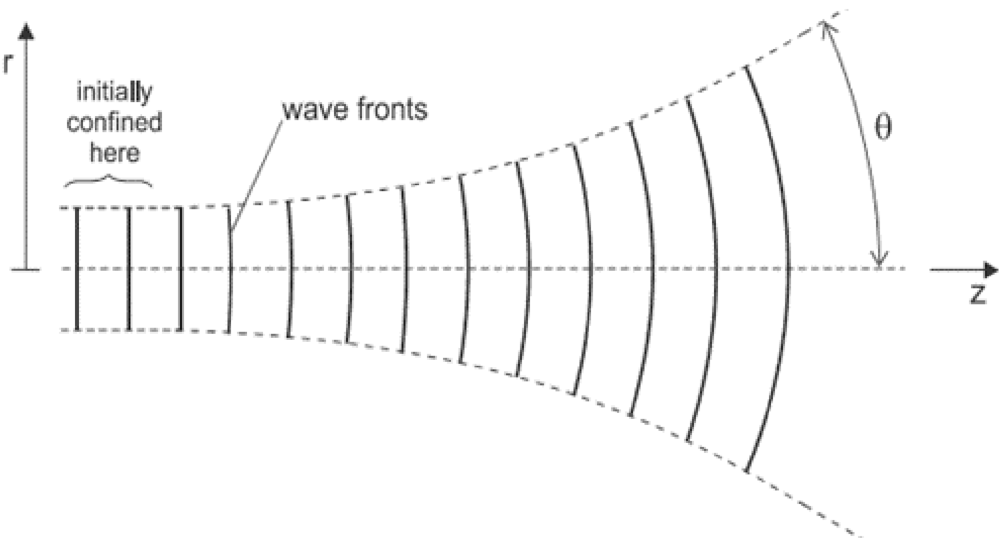

Fig.1 exhibits a typical gaussian beam, where r represents the radial distance from the z axis [5].

The electric field distribution at any arbitrary position along the z-axis is given by

$$E(r,z) = E_0 \frac{w_0}{w(z)} \exp\left(-\frac{r^2}{w(z)^2}\right), \tag{1}$$

where

- r is the radial distance from the z axis as shown in Fig.1;
- z specifies the position along the z-axis;
- E_0 is the magnitude of the electric field when $(r,z) = (0,0)$;

- The spot size $w(z)$ is the radius at which the electric field magnitude is equal to the product of the maximum electric field found on the distribution suggested by equation (1) times a factor of $1/e$,
- w_0, known as the waist radius, is the value of $w(z)$ at $z = 0$.

The electric field distribution at any arbitrary position z described by equation (1) is known as the Gaussian profile, which has the same shape as shown in Fig.2.

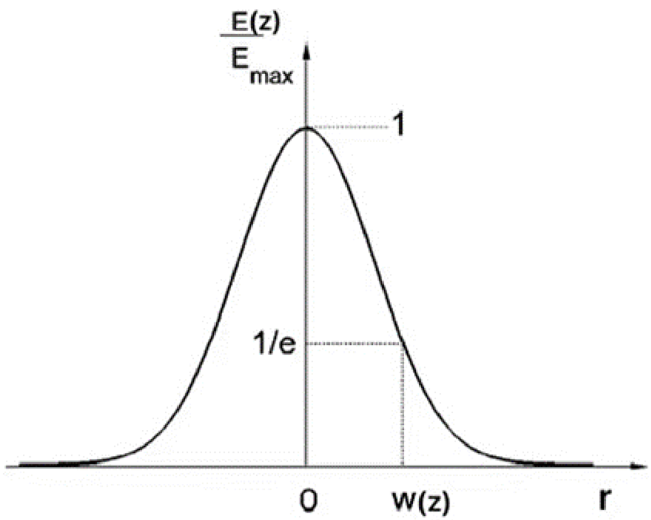

Fig.2 shows a normalized Gaussian profile, that is, the E v.s. r diagram of equation (1) *that has both sides divided by the maximum electric field strength. One can read the spot size corresponding to $1/e$ on the horizontal axis. The Gaussian profile has the same shape as the normalized one despite the different scaling.*

Given the waist radius w_0 and the wavelength of Gaussian beam λ, the spot size at any arbitrary position z can be computed by

$$w(z) = w_0 \sqrt{1 + \left(\frac{z}{z_0}\right)^2}, \tag{2}$$

where the Rayleigh range $z_0 = \frac{\pi w_0}{\lambda}$.

With z_0, the radius of wavefronts (curvature) as the ones shown in Fig.1, denoted by $R(z)$, can be computed by

$$R(z) = z\left(1 + \left(\frac{z}{z_0}\right)^2\right). \tag{3}$$

All in all, the position z and the waist radius will allow us to gain almost all the information regarding a Gaussian beam of a given wavelength.

The reminder of this page is left blank intentionally.

2.2 Diffraction

Diffraction refers to the phenomenon in which a mechanical or electromagnetic wave spreads out and forms some white and black bands on the screen after it penetrates through a slit or pass around an obstacle. In that sense, the Gaussian beam itself is a result of diffraction.

Suppose there is a beam of light striking on a slit or an obstacle with a length of W as shown in Fig.3.

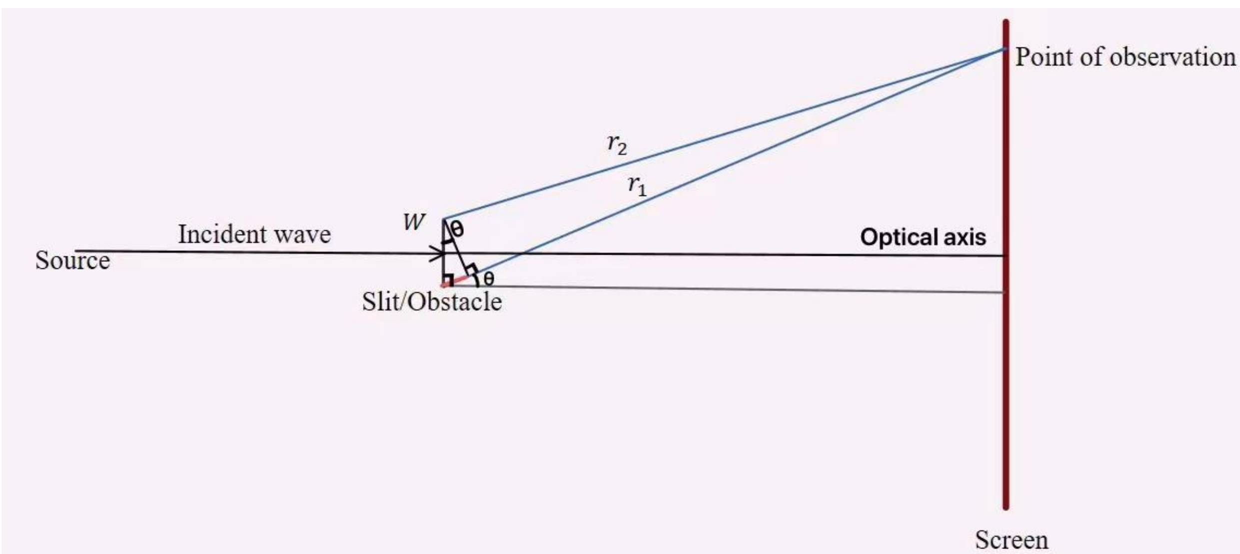

Fig.3 shows a beam of light from a source hitting on a slit or an obstacle.

At two ends of the slit are two diffracted wave paths coming to the same point of observation which have lengths of r_1 and r_2 respectively. According to the cosine law, we have

$$r_2{}^2 = r_1{}^2 + W^2 - 2br_1 \cos\left(\frac{\pi}{2} - \theta\right) = r_1{}^2 + W^2 - 2Wr_1 \sin(\theta) \tag{4}$$

Rewriting (4), we have

$$r_2 = r_1 \left(1 + \frac{W^2}{r_1{}^2} + 2\frac{W}{r_1}\sin(\theta)\right)^{\frac{1}{2}} \tag{5}$$

Let $x = \frac{W^2}{{r_1}^2} + 2\frac{W}{r_1}\sin(\theta)$. By applying the binomial expansion $(1+x)^{\frac{1}{2}} = 1 + \frac{1}{2}x - \frac{1}{8}x^2 + O(x^3)$ to (5), we have

$$\begin{aligned} r_2 &= r_1\left(1 + \frac{1}{2}(\frac{W^2}{{r_1}^2} + 2\frac{W}{r_1}\sin(\theta)) - \frac{1}{8}\left(\frac{W^4}{{r_1}^4} + 4\frac{W^3}{{r_1}^3}\sin(\theta) + 4\frac{W^2}{{r_1}^2}\sin^2(\theta)\right) + \cdots\right) \\ &= r_1\left(1 + \frac{W}{r_1}\sin(\theta) + \frac{1}{2}\frac{W^2}{{r_1}^2}\left(1 - \sin^2(\theta)\right) - \frac{1}{2}\frac{W^3}{{r_1}^3}\sin(\theta) - \frac{1}{8}\frac{W^4}{{r_1}^4} + \cdots\right) \end{aligned} \tag{6}$$

Applying $\cos^2(\theta) = 1 - \sin^2(\theta)$ to (6), we have

$$\begin{aligned} r_2 &= r_1\left(1 + \frac{W}{r_1}\sin(\theta) + \frac{1}{2}\frac{W^2}{{r_1}^2}\cos^2(\theta) - \frac{1}{2}\frac{W^3}{{r_1}^3}\sin(\theta) - \frac{1}{8}\frac{W^4}{{r_1}^4} + \cdots\right) \\ &= r_1\left(1 + \frac{W}{r_1}\sin(\theta) + \frac{1}{2}\frac{W^2}{{r_1}^2}\cos^2(\theta) + O\left(\frac{W^3}{{r_1}^3}\right)\right) \end{aligned} \tag{7}$$

Ignoring terms that have an order higher than 3 and rewriting (7), we have

$$r_2 - r_1 \cong W\sin(\theta) + \frac{W^2}{2r_1}\cos^2(\theta) \tag{8}$$

Suppose the wave number of the incident wave is given by k, then

$$kr_2 - kr_1 \cong kW\sin(\theta) + \frac{kW^2}{2r_1}\cos^2(\theta) \tag{9}$$

Suppose the wavenumber is given by $k = \frac{2\pi}{\lambda}$, where λ is the wavelength.

Substituting $k = \frac{2\pi}{\lambda}$T into the last term of (9), we have

$$\frac{kW^2}{2r_1}\cos^2(\theta) = \frac{\pi W^2}{\lambda r_1}\cos^2(\theta) \tag{10}$$

If $\frac{W^2}{\lambda r_1} \ll 1$, (10) becomes

$$r_2 - r_1 \cong W\sin(\theta) \tag{11}$$

(11) tells the path difference (the length of the red line segment in Fig.3) and suggests that two diffracted wave paths are approximately parallel to each other. Such an approximation only holds for the diffraction. Hence, it is safe to draw a conclusion that the diffraction occurs when $\frac{W^2}{\lambda r_1} \ll 1$. We can further simplify the conclusion by replacing r_1 with L which is the smaller of two distances: one is the distance between the slit/obstacle and the observation screen, the other is the distance between the wave source and the slit/obstacle. Geometrical speaking, r_1 is always longer than L. If $\frac{W^2}{L\lambda}$ is much smaller than 1, then $\frac{W^2}{\lambda r_1}$ must be much smaller than 1. Hence, we can summarize that diffraction occurs when

$$\frac{W^2}{L\lambda} \ll 1. \tag{12}$$

Such a statement is known as Fraunhofer condition, which is the geometrical requirement for the (Fraunhofer) diffraction to occur. For the future discussion, we define the Fresnel number, denoted by F, as

$$F = \frac{W^2}{L\lambda}. \tag{13}$$

When F is greater than 1, the diffraction image on the screen is distinguishable. However, some slight fringes are still vague. When F is close to 1, i.e., $F \sim 1$, the fringes look more prominent. In addition, the diffraction image is more structured. Such a phenomenon is called Fresnel diffraction. Strictly speaking, the diffraction suggested by (12) is known as the Fraunhofer diffraction whose pattern spreading out considerably and bearing little or no resemblance to the slit or the obstacle as $F \ll 1$. Such a Fresnel number allows us to analyze the rod diffraction pattern in the Fraunhofer limit for this project.

2.3 Poisson Spot

A bright spot found at the center of a circular object's diffraction image on the screen is known as the Poisson Spot (Fig.4).

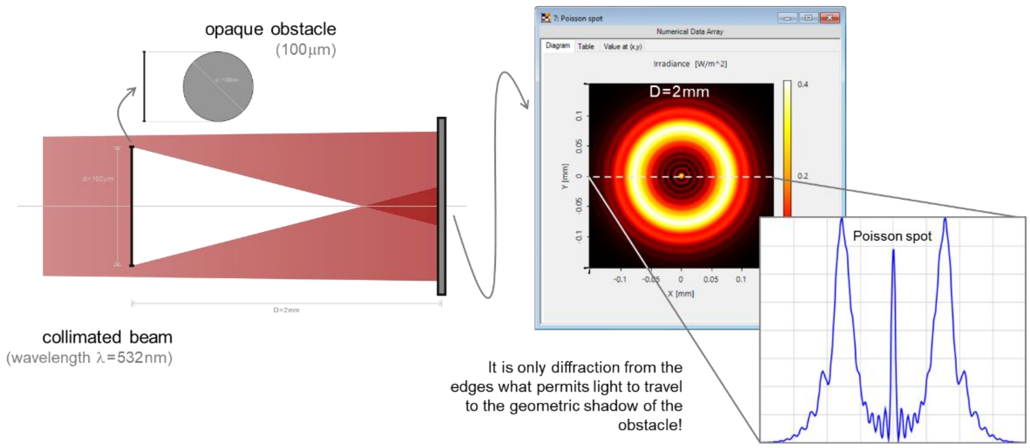

Fig.4 shows the Poisson spot found at the center of diffraction image on the screen when a collimated beam diffracts after it hits the opaque obstacle (https://www.lighttrans.com/use-cases/application/observation-of-the-poisson-spot.html).

In order for the Poisson spot to occur, the diffraction experiment should satisfy two conditions: one of which is $F = \frac{W^2}{L\lambda}$ greater than or equal to the value of 1 (W is the diameter of the circular object in this case), the other is that the edge of the circular object should be sufficiently smooth. We expected the Poisson spot to occur in the rod diffraction experiment in this project when the experimental conditions yield a Fresnel number that is close to one.

3. Methodology

In this project, we employed the Gaussian beam to conduct the rod diffraction experiment, that is, the diffraction by illuminating the rod with the Gaussian beam, to investigate what would its diffraction image look like. Fig.5 (a)&(b) below shows the experimental setup used to achieve such a goal.

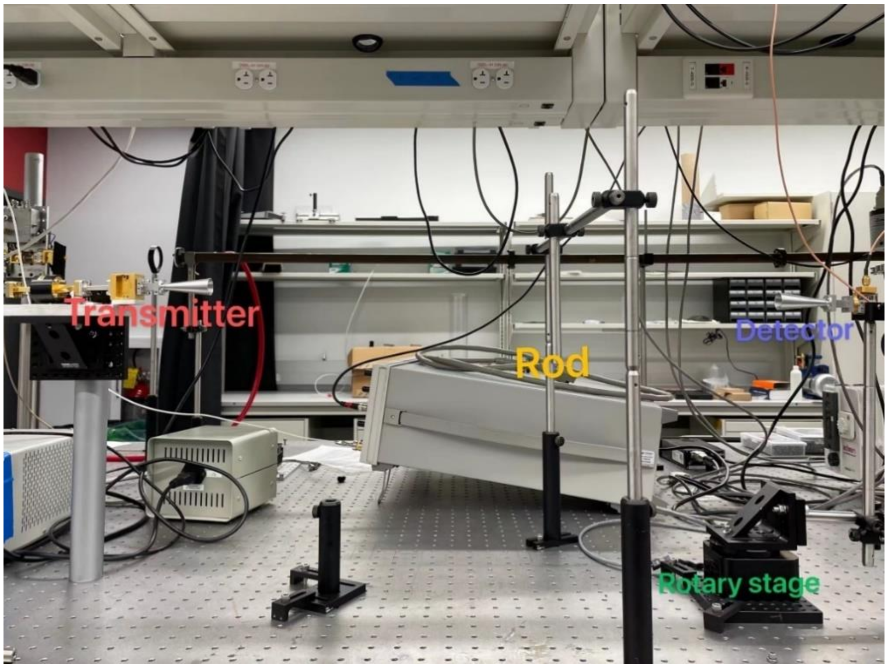

Fig.5(a) shows the side view of the experimental setup.

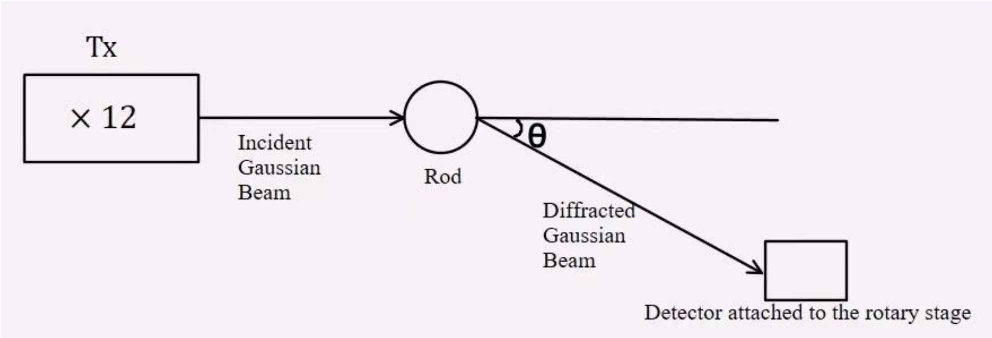

Fig.5(b) shows the bird's eye view of the experimental setup.

The experimental setup consisted of the transmitter (wave source), denoted by Tx in Fig. 5 (b), from which the millimeter-wave Gaussian beam is launched into free space, a rod whose diameter is 1.5 cm, and a detector (screen in this case) attached to the rotary stage. Most of the logistics of the experimental setup has no differences from typical diffraction experiments: the image is observed on the screen when the diffraction occurs as a result of the fact that the incident wave from the wave source hits the obstacle. In this case, the diffraction pattern is observed by the screen (a detector and analyzed with Igor Pro software in this case) when the diffraction occurs as a result of the fact that the incident Gaussian beam coming out of from the transmitter hits the rod. There are only two emphases about this experimental setup which are the transmitter and the detector.

The reminder of this page is left blank intentionally.

3.1 Transmitter

In this experiment, we planned to use 60, 90, and 120 GHz Gaussian beams. However, the signal generator in the lab is only able to generate signals whose frequency ranges from 10 kHz to 40 GHz. In order to solve such an issue, we used a millimeter-wave multiplier chain capable of amplifying the frequency by a factor of 12 before sending the signal out (Fig.6) such that we only needed to input 5, 7.5, and 10 GHz to generate Gaussian beams at the targeted frequencies. The Gaussian beam is launched from the conical horn shown in Fig. 6 where the horn's opening as a diameter of 1.0 cm and the beam divergence from the horn is approximately 10 degrees. The signal generator was amplitude modulated and the diode detector signal was connected to a lock-in amplifier to enhance the signal-to-noise of the system. The Gaussian beam divergence of ~10 degrees from the horn ensured the beam fully illuminated the target.

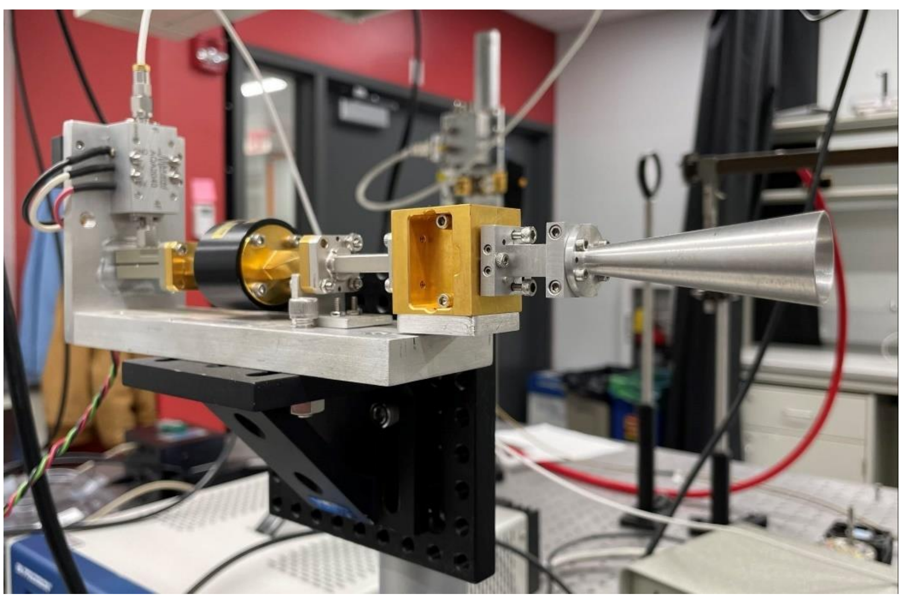

Fig.6 shows the generator used in the experimental setup. The signal for the function generator comes in through the white cable and the devices on the aluminum block amplify and multiply the frequency by ×12 before a Gaussian beam is launched by the conical horn that has a 1 cm aperture.

3.2 Rotary Stage

The 2.1 section of the background chapter suggests that the wavefronts of a Gaussian beam are curved. Hence, the detector was attached to a rotary stage which is able to sweep a whole angle of 60 degrees with the assistance of NI LabVIEW and automated DAQ so that the detector could collect the data (power) of each point on the curved wavefronts in the diffraction experiment (Fig.7). Additionally, the rotary stage ensures that the distance between the screen and the rod should always be constant. In order to make the detector rotate as continuously as possible, a whole swipe of 60 degrees was divided into 120 steps. In other words, 120 data points were collected on the wavefront. Igor Pro then could plot the diffraction pattern, i.e., power versus angle diagram, by feeding it the collected data.

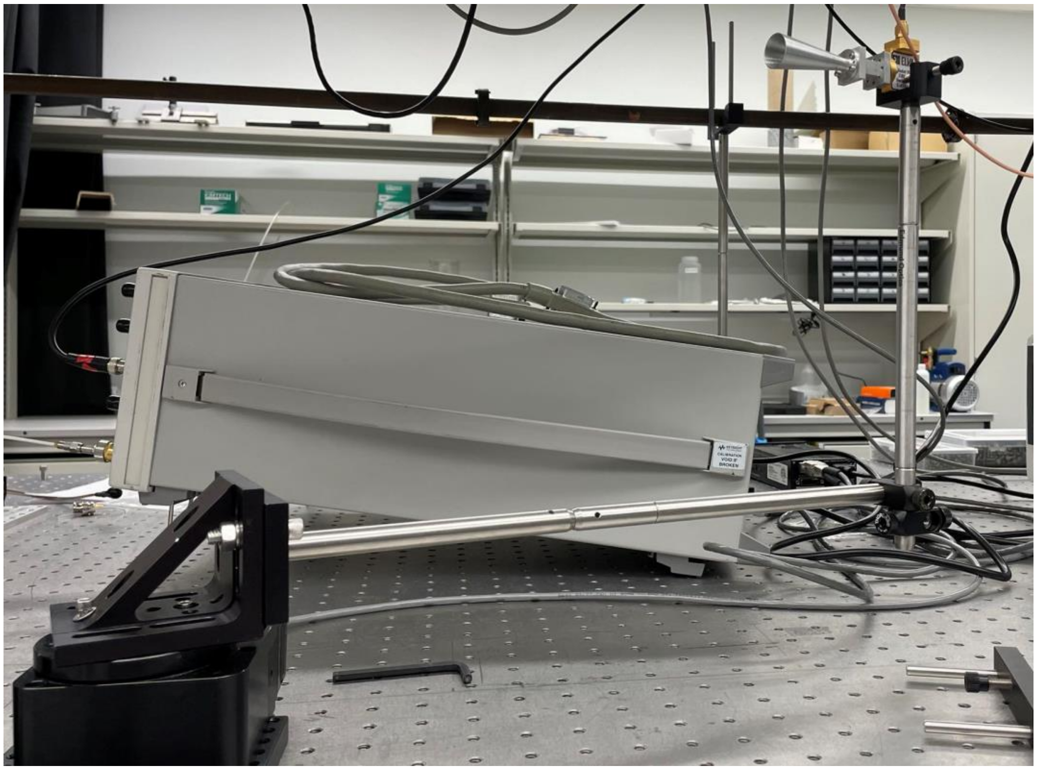

Fig.7 shows the detector attached to the rotary stage. The detector has a similar conical horn antenna with a 1 cm aperture.

4 Finding

This chapter is divided into two parts: the first part states the results of the rod diffraction experiment which employs the experimental setup described in the methodology chapter, and the second part analyzes these results by applying the theories in 2.2 and 2.3 sections of the background chapter.

4.1 Rod diffraction pattern

Given that the distance between the transmitter and the rod was constant ($48.6\ cm$) throughout the whole experiment, the rod diffraction was repeated with three different frequencies, i.e., 60, 90, and 120 GHz. For each of these frequencies, the rod diffraction was repeated with four different distances between the rod and the detector, i.e., 9.5, 22, 31, and 39.5 cm. Fig. 8~10 exhibit the results (diffraction patterns) of the experiment.

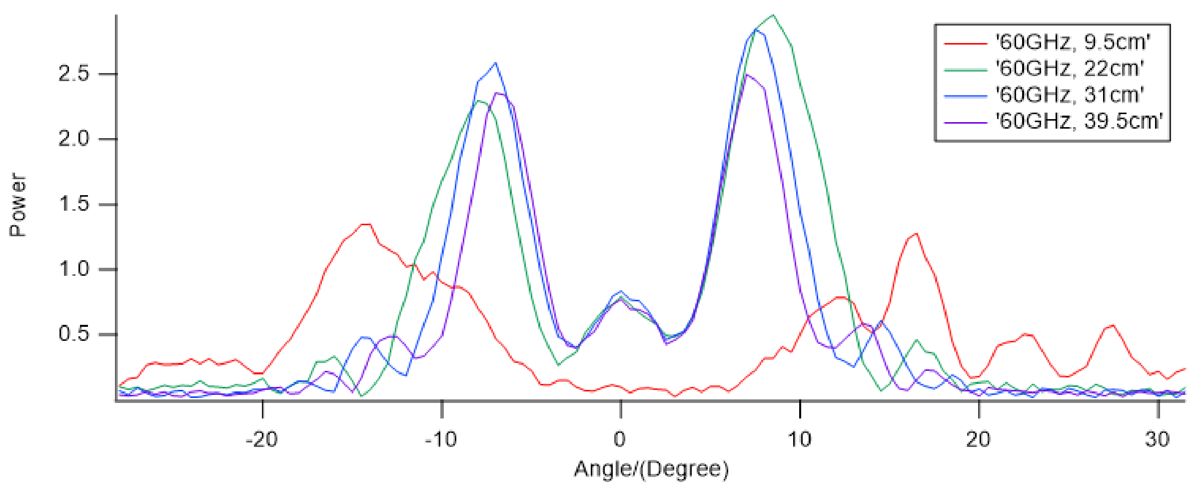

Fig.8 shows the rod diffraction patterns of the 60 GHz Gaussian beam with different distances between the rod and the detector.

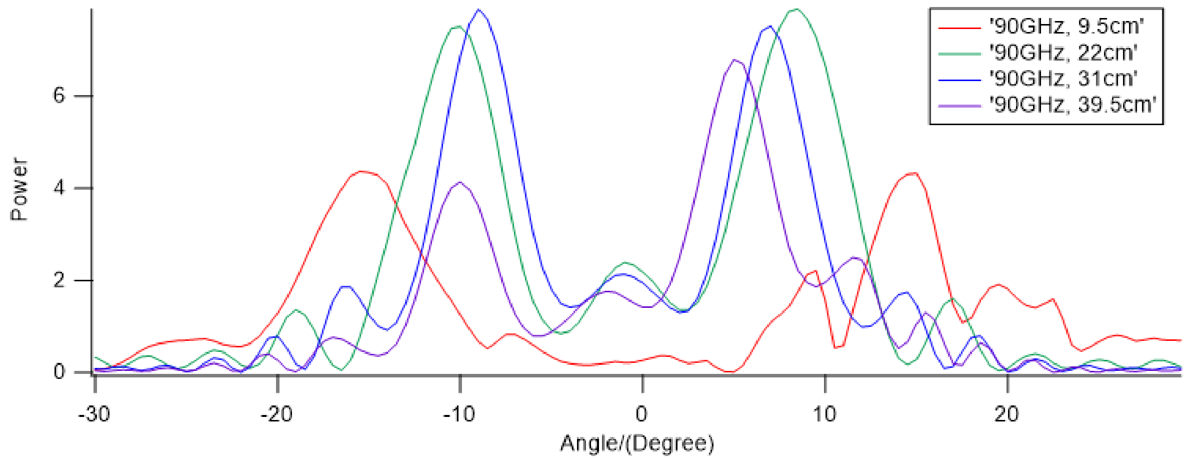

Fig.9 shows the rod diffraction patterns of the 90GHz Gaussian beam with different distances between the rod and the detector.

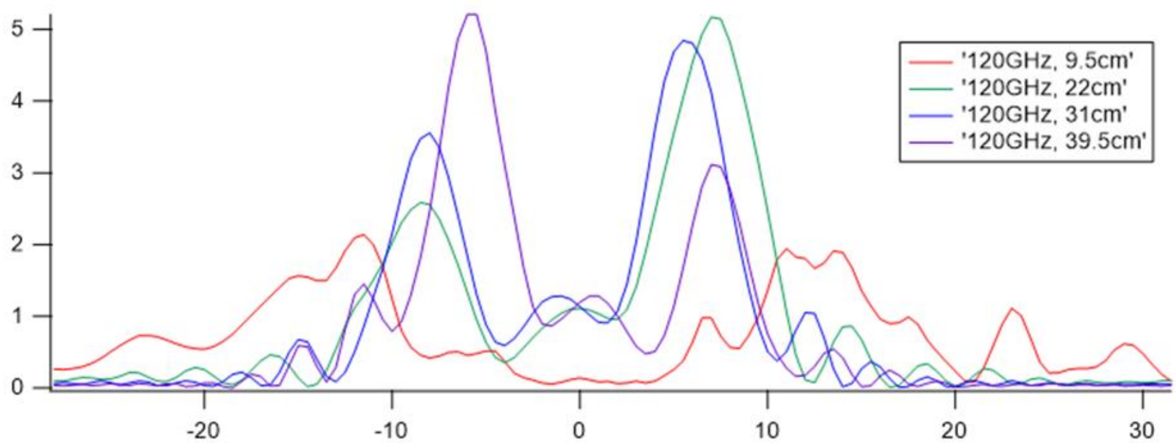

Fig.10 shows the rod diffraction patterns of the 120GHz Gaussian beam with different distances between the rod and the detector.

4.2 Analysis

Given that the diameter of the rod equals 1.5 cm, one can compute the Fresnel numbers for all diffraction patterns in the last section. In the computation, L is the distance between the rod and the detector since 9.5, 22, 31, and 39.5 cm are all smaller than the distance between the transmitter and the rod which is 48.6 cm. Tables 1 presents all Fresnel numbers F of diffraction patterns subject to their corresponding frequency and L.

$L/(m)$	$F\ (60\ GHz)$	$F\ (90\ GHz)$	$F\ (120\ GHz)$
$0.095\ m$	0.47	0.71	0.95
$0.22\ m$	0.20	0.31	0.41
$0.31\ m$	0.15	0.22	0.29
$0.395m$	0.11	0.17	0.23

Table 1 shows the Fresnel numbers of the rod diffraction patterns using 60, 90, and 120 GHz Gaussian beams with different distances between the rod and the detector.

These data are certainly mind-blowing. At first hand, I thought there exists a Poisson spot for all situations based on the fact that there is a small but noticeable power at the center of all diffraction patterns subject to their corresponding frequency and L presented in section 4.1. Additionally, the rod is sufficiently smooth. However, Fresnel numbers of all diffraction patterns have a value of less than 1, which indicates that they are all the Fraunhofer diffraction limit. Recall from section 2.3 that the Poisson spot only occurs when there is a Fresnel diffraction; that is, $F \geq 1$. Hence, we can conclude that there is no Poisson spot for all diffraction patterns, though there exists some power at the center of all diffraction patterns. These Fresnel numbers still make sense since the two sides of the diffraction diverges out as we move the detector further away from the rod (F becomes gradually smaller as the detector moves away from the rod for all frequencies). In a meanwhile, for each frequency, the diffraction pattern around the center looks very blurry when $L = 22\ cm$ but starts to become clearer and more prominent as the detector moves further away from the rod. Both phenomena satisfy the description of Fraunhofer diffraction in section 2.2.

Theoretical speaking, the power at the Poisson spot should be higher than the most part of the diffraction pattern. To study such an interesting phenomenon, it is worth and without the loss of the generality to have a look at the case of the diffraction patterns using the 120 GHz Gaussian beam since its largest Fresnel number is very close to 1 and is the best experimental conditions to the requirement for the Poisson spot to occur. Theory in section 2.2 suggests that the diffraction pattern will bear little or no resemblance to the slit or the obstacle as $F \ll 1$. In such a case, F is smaller than 1, but not much smaller than 1 (especially when $F = 0.95$). One possible explanation is that we measured the diffraction patterns when there was a transition from the Fresnel diffraction to the Fraunhofer diffraction. As a result, the appearance of the Poisson spot starts to collapse down as the detector moves further away from the rod. An additional consideration is the angular resolution of our system. The aperture of the horn is 1 cm and limits the angular resolution of the system. In the case when $F = 0.95$, the distance from the rod to the detector horn is 9.5 cm. The angular resolution is the diameter of the horn to the distance from the rod to the detector gives an angular resolution of ~6 degrees, which will likely ‘blur’ the measurement of the Poisson spot. As the detector moves out to a distance of 39.5 cm, the angular resolution improves to ~1.5 degrees, but the Fresnel number decreases from ~1 to 0.23 and the prominence of the Poisson spot will decrease as it enters the Fraunhofer diffraction limit.

5 Discussion

At the end of chapter 4, we come to a hypothesis that we conducted the diffraction experiment when there was a transition from the Fresnel diffraction to the Fraunhofer diffraction. To verify such an idea, the future work can be done by doing the rod diffraction experiment with more different values of L such that $F \geq 1$ to see whether there will be a Poisson spot at the center of the diffraction pattern. One easy way to do that is to adjust the distance between the transmitter and the rod such that it becomes the smaller of two distances. We can certainly adjust the distance between the rod and the detector. However, the rotary stage should stand right beneath the rod such that we can make sure the detector is always aiming at the rod during rotation, which means the arm of the rotary stage is not long enough to create more different values of L. Actually, 9.5cm cm and 39.5 cm are the closest and furthest distances between the rod and the detector respectively. There seems to be clear evidence of the Poisson spot (peak intensity in the 'shadow' of the rod directly behind it), but the characteristics did not follow our expectations as a function of the Fresnel number.

The primary goal of this project was to develop the system to measure the scattering and diffraction patterns in the millimeter-wave region. Figures 8-10 show clear evidence of diffraction patterns such as the Poisson spot and secondary maximum. However, the experimental system has competing tradeoff in terms of angular resolution and the Fresnel number of the experimental set up. The system is at the stage to begin to analyze the current data sets in the context of Fresnel and Fraunhofer diffraction and to investigate modifications of the experimental set up to further experimental distinguish these two regions.

Recall the application of the car radar system in the introduction chapter. It is essential to understand how milli-meter wave behaves when it hits an object in front of the car. However, one practical problem that raises in real-life is that how will the car radar system receive the information of the milli-meter wave diffraction behavior since there will not be a detector behind the object on a highway. Another suggested future work can be studying the reflection behavior of the milli-meter wave.

Reference

[1] Goulianos, Angelos A., et al. "Measurements and characterisation of surface scattering at 60 GHz." *2017 IEEE 86th Vehicular Technology Conference (VTC-Fall)*. IEEE, 2017.

[2] Li, Eric S., and Kamal Sarabandi. "Low grazing incidence millimeter-wave scattering models and measurements for various road surfaces." *IEEE Transactions on Antennas and Propagation* 47.5 (1999): 851-861.

[3] Petkie, Douglas T., et al. "Active and passive imaging in the THz spectral region: phenomenology, dynamic range, modes, and illumination." *JOSA B* 25.9 (2008): 1523-1531.

[4] Järveläinen, Jan, et al. "60 GHz radio wave propagation prediction in a hospital environment using an accurate room structural model." *2012 Loughborough Antennas & Propagation Conference (LAPC)*. IEEE, 2012.

[5] Quimby, Richard S. *Photonics and lasers: an introduction*. John Wiley & Sons, 2006.

[6] Hecht, Eugene. *Optics, 5e*. Pearson Education India, 2002.